THE JOURNAL OF BIOLOGICAL CHEMISTRY VOL. 284, NO. 16, pp. 10793–10807, April 17, 2009


# Neuronal Nogo-A Modulates Growth Cone Motility via Rho-GTP/LIMK1/Cofilin in the Unlesioned Adult Nervous System*[S]

Received for publication, October 29, 2008, and in revised form, February 4, 2009 Published, JBC Papers in Press, February 9, 2009, DOI 10.1074/jbc.M808297200

**Laura Montani**[‡§1], **Bertran Gerrits**[¶], **Peter Gehrig**[¶], **Anissa Kempf**[‡§], **Leda Dimou**[‡§2], **Bernd Wollscheid**[‖], **and Martin E. Schwab**[‡§]

*From the* [‡]*Brain Research Institute and* [¶]*Functional Genomics Center, University of Zurich, and the* [§]*Department of Biology, ETH Zürich, 8057 Zurich, Switzerland and the* [‖]*Molecular Systems Biology Institute, ETH Zürich, 8093 Zurich, Switzerland*

**Nogo-A has been extensively studied as a myelin-associated neurite outgrowth inhibitor in the lesioned adult central nervous system. However, its role in the intact central nervous system has not yet been clarified. Analysis of the intact adult nervous system of C57BL/6 Nogo-A knock-out (KO) *versus* wild-type (WT) mice by a combined two-dimensional gel electrophoresis and isotope-coded affinity tagging approach revealed regulation of cytoskeleton-, transport-, and signaling growth-related proteins, pointing to regulation of the actin cytoskeleton, the neuronal growth machinery, and in particular the Rho-GTPase/LIMK1/cofilin pathway. Nogo-A KO adult neurons showed enlarged, more motile growth cones compared with WT neurons. The phenotype was reproduced by acute *in vitro* neutralization of neuronal Nogo-A. LIMK1 phosphorylation was increased in Nogo-A KO growth cones, and its reduction caused the decrease of KO growth cone motility to WT levels. Our study suggests that in the unlesioned adult nervous system, neuronal Nogo-A can restrict neuronal growth through negative modulation of growth cone motility.**

During postnatal development, central nervous system (CNS)[3] neurons lose their ability to regenerate in part due to the presence of neurite outgrowth inhibitors, *e.g.* in myelin or in the glial scar (1, 2). A number of molecules with suggested growth inhibitory activity are present in the adult CNS: Nogo-A, oligodendrocyte myelin glycoprotein, myelin-associated glycoprotein, repulsive guidance molecule (2–4), and certain ephrins (5, 6), semaphorins (7–9) and proteoglycans (1). Nogo-A has been extensively studied for its role in inhibiting axonal regeneration as well as compensatory fiber growth in the injured adult CNS *in vivo* (2, 4, 10). Neutralization of Nogo-A through *in vivo* application of function-blocking antibodies induces neuronal growth after spinal cord or brain injury in adult rodents as well as primates (2, 11). A moderate increase in regeneration and compensatory fiber growth after lesion has been also observed in Nogo-A knock-out (KO) mice at different degrees depending on intrinsic genetic differences in the different mouse strains analyzed (10, 12–15). In the adult CNS, Nogo-A is found predominantly in the innermost adaxonal and outermost myelin membranes and in oligodendrocytes (16, 17). During development, Nogo-A is expressed in neurons, where it has been suggested to play a role in neuronal migration and cortical development (18) and to regulate synaptic plasticity (19–21). Neuronal expression of Nogo-A is down-regulated following the onset of myelination but persists at higher levels in particular neuronal populations such as in the hippocampus (16, 22), olfactory bulb, deep cerebellar nuclei, spinal motor neurons (23), and dorsal root ganglia (DRG) (24). The possible roles of neuronal Nogo-A in the intact adult CNS have not been studied in detail. It has been shown that its neutralization *in vivo* in intact adult rats produces a transitory growth response of Purkinje axons and the corticospinal tract (25–27).

In the last few years, the application of systems biology approaches based on large-scale analysis of proteins has been successfully applied to complex biological networks, *e.g.* for the analysis of neurodegenerative disorders and infections (28, 29). In this study, we used systems biology profiling based on two proteomic approaches (two-dimensional gel electrophoresis and isotope-coded affinity tagging (ICAT)) to address the role of Nogo-A in the unlesioned adult CNS. We compared the adult CNS of C57BL/6 naïve, unlesioned, Nogo-A KO and wild-type (WT) mice, and using a combination of approaches, we report that the depletion of Nogo-A or functional blockade of neuronal Nogo-A in the adult as well as postnatal intact nervous system causes the reorganization of the cytoskeletal growth cone machinery at both the molecular and morphological levels and that the LIMK1/cofilin phosphorylation state is critical for this process.

* This work was supported by Swiss National Science Foundation Grant 31-63633.00, the National Center of Competence in Research "Neural Plasticity and Repair" of the Swiss National Science Foundation, the Spinal Cord Consortium of the Christopher and Dana Reeve Foundation (Project MSC 2005(1)), the Transregio-Sonderforschungsbereich Konstanz-Zurich (Project 34150609), and the NeuroNe Network of Excellence of the European Consortium for Research in Neurodegenerative Diseases (Sixth Framework Programme).

[S] The on-line version of this article (available at http://www.jbc.org) contains supplemental Figs. 1–4, Tables 1 and 2, and Videos 1 and 2.

[1] To whom correspondence should be addressed: Brain Research Inst., Winterthurerstr. 190, 8057 Zurich, Switzerland. Fax: 41-44-635-3303; E-mail: montani@hifo.uzh.ch.

[2] Present address: Physiologisches Inst., Physiologische Genomik-Ludwig-Maximilian-Universitaet, 80336 München, Germany.

[3] The abbreviations used are: CNS, central nervous system; KO, knock-out; DRG, dorsal root ganglia/ganglion; ICAT, isotope-coded affinity tagging; WT, wild-type; CHAPS, 3-[(3-cholamidopropyl)dimethylammonio]-1-propanesulfonic acid; MALDI, matrix-assisted laser desorption ionization; HPLC, high performance liquid chromatography; P0, postnatal day 0; NGF, nerve growth factor.

## EXPERIMENTAL PROCEDURES

*Animals*—Male C57BL/6 Nogo-A KO mice with a strain purity of >99.98% and back-crossed for >10 generations (12) and male C57BL/6 WT mice were used. All animal experiments were performed with the approval of and in strict accordance with the guidelines of the Zurich Cantonal Veterinary Office. All efforts were made to minimize animal suffering and to reduce the number of animals required.

*Antibodies*—Rabbit anti-cofilin (Western blot, 1:1000; Chemicon), rabbit anti-phospho-cofilin $Ser^3$ (Western blot, 1:1000; Chemicon), mouse anti-glyceraldehyde-3-phosphate dehydrogenase (Western blot, 1:15000; Abcam), rabbit anti-LIMK1 (Western blot, 1:1000; immunocytochemistry, 1:100; Abcam), mouse anti-Nogo-A 11C7 (Western blot, 1:15000; neutralization assay, 3 $\mu$g/ml; Novartis), rabbit anti-phospho-LIMK1 $Thr^{508}$ (Western blot, 1:1000; immunocytochemistry, 1:150; Abcam), rabbit anti-$\beta$-tubulin (immunocytochemistry, 1:150; Abcam), mouse anti-$\beta$-tubulin III (immunocytochemistry, 1:2000; Promega), horseradish peroxidase-coupled goat anti-mouse IgG (Western blot, 1:15000; Pierce), Cy3-coupled goat anti-rabbit IgG (H+L; immunocytochemistry, 1:3000; Jackson ImmunoResearch Laboratories), horseradish peroxidase-coupled donkey anti-rabbit IgG (Western blot, 1:10000; Pierce), rabbit IgG (Western blot, 1:1000; Pierce), Alexa 488-conjugated phalloidin (immunocytochemistry, 1:40; Molecular Probes), glutathione *S*-transferase-tagged rhothekin Rho-binding domain protein (1:100; Cytoskeleton Inc.) antibodies and rabbit anti-glutathione *S*-transferase polyclonal antibody (1:1000; Abcam) were from the indicated manufacturers.

*Two-dimensional Gel Electrophoresis*—Lumbar spinal cords of three adult Nogo-A KO and WT mice were dissected and transferred to CHAPS lysis buffer (50 mM $NaH_2PO_4$ (pH 8.0), 150 mM NaCl, 0.5% CHAPS, protease inhibitor mixture (Roche Applied Science)) on ice. Tissues were disrupted using a rotor-stator homogenizer. After 30 min on ice, samples were centrifuged (15 min, 2000 × *g*, 4 °C), and the total protein concentration of the supernatant was determined using a NanoDrop Technologies spectrophotometer system. Each sample was processed independently to permit evaluation of individual differences. 150 $\mu$g of proteins/sample was loaded onto 3–10 and 4–7 IPG strips (Amersham Biosciences) in rehydration solution (7 M urea, 2 M thiourea, 2% CHAPS, 0.3% dithiothreitol, and 3–10 or 4–7 IPG buffer (Amersham Biosciences)). IPG strips were refocused and transferred onto 11% SDS-polyacrylamide gels. The second dimension was resolved in SDS electrophoresis buffer in an Ettan DALT*twelve* system (GE Healthcare) according to system instructions. Protein spot staining was performed with SYPRO Ruby (Molecular Probes) according to the manufacturer's protocol. Images were captured using a Typhoon 9400 scanner (GE Healthcare) and analyzed with Proteomweaver software (Version 2.2; Definiens). A protein target excision list of the regulated spots (one-way analysis of variance, $p \leq 0.05$) was generated, and spots were excised with a GelPix spot picking robot (Genetix) and processed for in-gel digestion, extraction, and purification of the peptides as well as spotting onto MALDI target plates using a Tecan Genesis ProTeam 150 digester/spotter running under Gemini software. Samples were analyzed on an Applied Biosystems 4700 proteomics analyzer MALDI TOF/TOF system. All mass spectra were recorded in positive reflector mode, and they were generated by accumulating data from 5000 laser pulses. Up to five spectral peaks/spot were included in the list for the acquisition of tandem mass spectra. GPS Explorer Software Version 2.0 (Applied Biosystems) was used for submitting mass spectrometry and tandem mass spectrometry data for data base searching. Mascot (Matrix Science) was utilized as the search engine. A mouse protein data base from the European Bioinformatics Institute (33081 sequences; release date, March 19, 2005) was used.

*ICAT*—Lumbar spinal cords of three adult Nogo-A KO as well as WT mice were dissected. Because of technical restrictions, tissues from the same genotype were pooled, transferred to lysis buffer (5 mM EDTA, 50 mM Tris-HCl (pH 8.3), 1% RapiGest (Waters Corp.)), and disrupted using a rotor-stator homogenizer. After 30 min on ice, samples were centrifuged (15 min, 2000 × *g*, 4 °C), and the total protein concentration of the supernatant was determined using a NanoDrop Technologies spectrophotometer system. 600 $\mu$g of both samples were reduced with tributylphosphine and labeled with ICAT reagents (Applied Biosystems) for 2 h at 37 °C. After quenching with dithiothreitol, samples were combined and digested with trypsin overnight at 37 °C. The peptide mixture was fractionated by HPLC in a KCl gradient. Biotinylated peptides were purified on Applied Biosystems ICAT avidin cartridges according to the manufacturer's protocol. Fractions were dried by speed-vacuuming, biotin-cleaved with Applied Biosystems cleaving reagents, and cleaned with Sep-Pak cartridges (Vac C18, 1 cc; Waters Corp.). ICAT peptides were analyzed by nano-liquid chromatography/mass spectrometry using an LTQ FT mass spectrometer (Thermo Electron Corp.). Peptides were separated on a nano-HPLC system (Agilent Technologies) online prior to mass spectrometry analysis on a homemade $C_{18}$ reversed-phase column (Magic, 5 $\mu$m, 100A $C_{18}$ AQ; Michrom) using an acetonitrile/water system at a flow rate of 200 nl/min. Tandem mass spectra were acquired in a data-dependent manner. Typically, four tandem mass spectrometries were performed after each high accuracy spectral acquisition range survey. Data analysis was performed through the Sisyphus platform (developed by the group of B. W.); ProteinProphet probability score and ASAPRatio were applied.

*Dissociated DRG*—DRG from three postnatal day 0 (P0) and three adult KO and WT mice per experiment were dissected and trypsinized at 37 °C. After trituration, cells were filtered, plated at low density ($1.5 \times 10^4$, glass coverslips coated with 20 $\mu$g/ml poly-L-lysine and 5 $\mu$g/ml laminin), and cultured (L-15 medium with L-glutamine, N1 additives, 50 $\mu$g/ml nerve growth factor (NGF), and 0.25% $NaHCO_3$ at 5% $CO_2$ and 37 °C) for 6 h (P0) or 14 h or 1–3 days *in vitro* (adult). Each experiment was repeated three times with four experimental replicates each unless indicated otherwise.

Parameters of neuronal morphology (branching points, number of neurites, number of filopodia, lamellipodial area, lamellipodial perimeter, tubulin-containing core area) were measured using ImageJ software (National Institutes of Health) in 20 neurons per experiment in three independent experi-

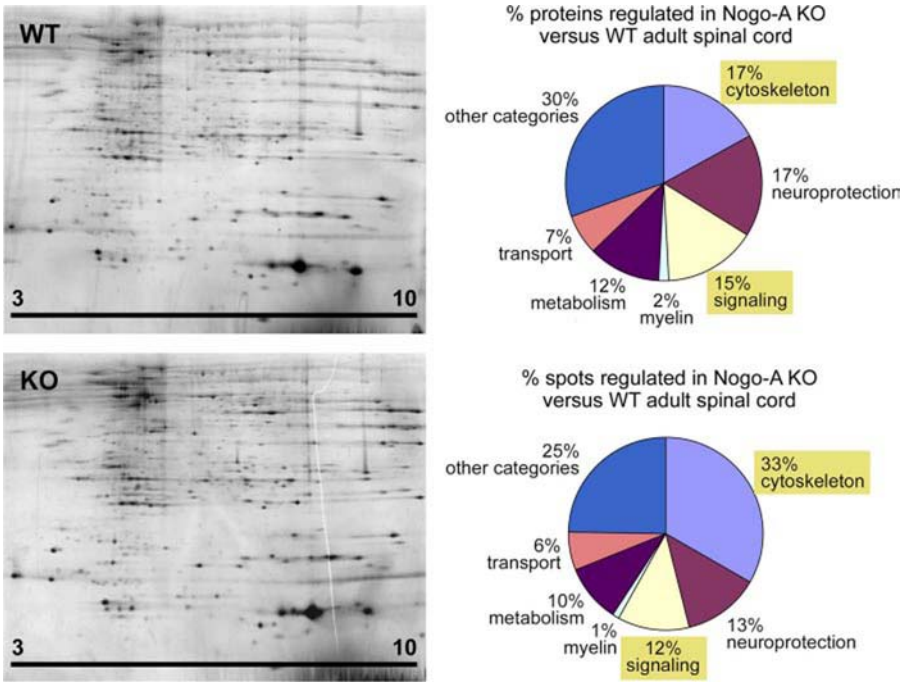


FIGURE 1. **Protein expression changes in Nogo-A KO *versus* WT adult mouse spinal cord as shown by two-dimensional gels.** Representative images show spinal cord proteins of WT and Nogo-A KO mice separated on pH 3–10 isoelectrofocusing strips and 11% SDS-polyacrylamide two-dimensional gels. Shown is the percentage of identified proteins per total identified proteins and spots in each functional category (calculated from the total number of proteins (62) and spots (93), respectively) differentially expressed in Nogo-A KO *versus* WT adult spinal cord. Assignment to functional categories was made on the basis of GeneOntology and literature mining.

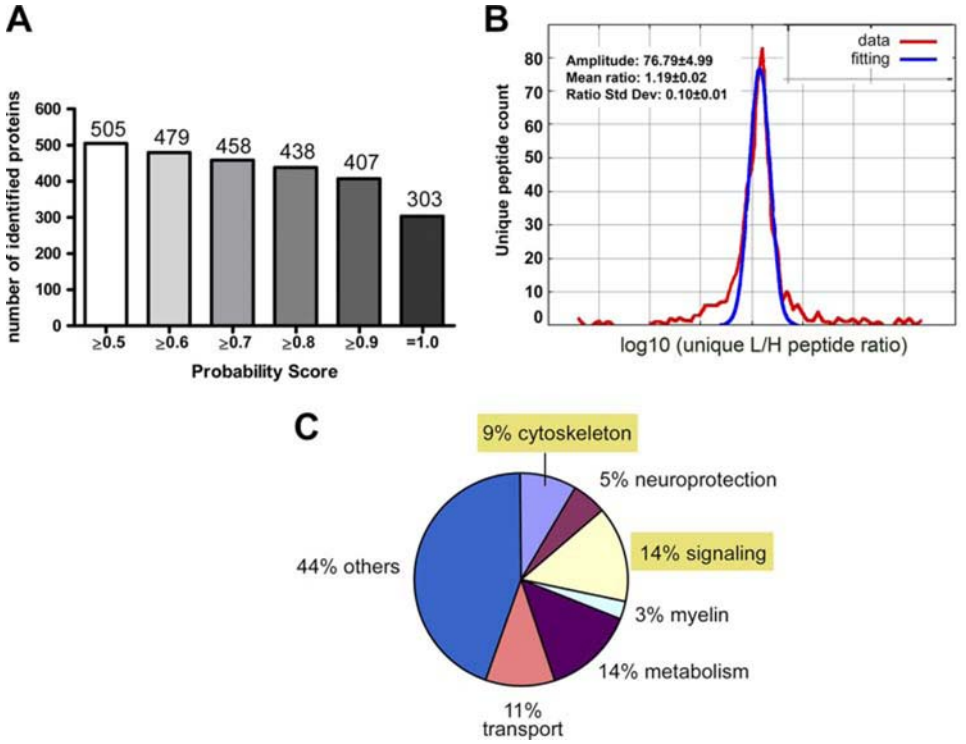


FIGURE 2. **Quantitative proteomic analysis of Nogo-A KO *versus* WT adult mouse spinal cord by ICAT analysis.** *A*, number of identified proteins (505, 479, 458, 438, 407, and 303) according to different ProteinProphet probability scores (from ≥0.5 to 1.0). *B*, logarithmic distribution of the number of identified proteins (407 proteins total; $p \geq 0.9$) as a function of the observed -fold change values. The data presented a normal distribution around a mean ratio of 1.19 ± 0.02; this value was used to normalize the -fold change values. *Std Dev*, standard deviation; *L/H*, light/heavy. *C*, percentage of proteins in each functional category differentially expressed in Nogo-A KO *versus* WT adult spinal cord. Assignment to functional categories was made on the basis of Panther analysis and literature mining.

ments for a total of 60 neurons. The percentage of enlarged growth cones and growth cone morphology were assessed for all growth cones of the total number of neurons in three independent experiments. The total length of the neurite tree was measured using Metamorph software (Molecular Devices). The parameters of neuronal morphology for P0 dissociated DRG were measured using ImageJ software in at least 10 neurons per coverslip in four coverslips (experimental replicates) in two separate experiments for a total of at least 80 neurons. P0 neurons were manually traced using ImageJ software with the NeuronJ plug-in (30). Data analysis was performed using Prism 4.0 (GraphPad Software).

*Nogo-A Neutralization*—Highly purified mouse anti-Nogo-A monoclonal antibody 11C7 or a control highly purified mouse IgG antibody (3 μg/ml) was applied to Nogo-A KO and WT adult low density dissociated DRG neurons at plating time. Cells were cultured for 14 h. Each experiment was repeated three times, with four experimental replicates each. The percentage of enlarged growth cones was calculated for the total number of neurons in three independent experiments. Data analysis was performed using Prism 4.0.

*COS-7 Cultures*—Native COS-7 cells were cultured overnight in Dulbecco's modified Eagle's medium, 10% fetal bovine serum, and 1% gentamicin and then treated for 1 h with increasing concentrations (5, 10, 20, and 40 μg/ml) of the S3 peptide or reverse-sequence control RV peptide.

*PC12 Cultures*—PC12 cells were cultured for 3 days in Dulbecco's modified Eagle's medium, 6% horse serum, 6% newborn calf serum, and 1% penicillin/streptomycin. Following trypsinization, cells were counted and plated on poly-L-lysine-coated coverslips (20 μg/ml) at a density of 50,000 cells/100 μl in differentiating medium (Dulbecco's modified Eagle's medium, 1% bovine serum albumin, and 100 ng/ml NGF). Cells were cultured for

**TABLE 1**

**Two-dimensional gel electrophoresis spots differentially expressed in the spinal cords of Nogo-A KO *versus* WT mice in the cytoskeleton and signaling categories**

GFAP, glial fibrillary acidic protein; PKC, protein kinase C; FGF, fibroblast growth factor.

| Spot No. | Protein[a] | Mean change ($p \leq 0.05$) | IPG strip |
|---|---|---|---|
| | | *-fold* | |
| **Cytoskeleton** | | | |
| 1837 | Actin ($\beta$, $\gamma$, $\alpha$) | 0.76 | 4–7 |
| 1926 | $\alpha$-Centractin (actin-related protein 1) | 1.22 | 4–7 |
| 2032 | $\alpha$-Internexin (66-kDa filament) | 0.05[b] | 4–7 |
| 2155 | $\alpha$-Internexin (66-kDa filament) | 20.00[b] | 4–7 |
| 2147 | $\alpha$-Internexin (66-kDa filament) | 20.00[b] | 4–7 |
| 4102 | Cofilin, non-muscle isoform (cofilin-1) | 0.79 | 3–10 |
| 4180 | Cofilin, non-muscle isoform (cofilin-1) | 1.70 | 3–10 |
| 4173 | GFAP | 1.50 | 3–10 |
| 4505 | GFAP | 20.00[b] | 3–10 |
| 4526 | GFAP | 20.00[b] | 3–10 |
| 3951 | GFAP | 1.92 | 3–10 |
| 4502 | GFAP | 20.00[b] | 3–10 |
| 4058 | GFAP | 1.50 | 3–10 |
| 1864 | GFAP | 2.94 | 4–7 |
| 2027 | GFAP | 0.60 | 4–7 |
| 2038 | GFAP | 0.05[b] | 4–7 |
| 2018 | GFAP | 0.60 | 4–7 |
| 4007 | Neurofilament-68 | 0.63 | 3–10 |
| 4339 | Neurofilament-68 | 0.05[b] | 3–10 |
| 1679 | Neurofilament-68 | 0.62 | 4–7 |
| 1674 | Neurofilament-68 | 0.62 | 4–7 |
| 1753 | Neurofilament-68 | 1.50 | 4–7 |
| 4119 | Myosin regulatory light chain 2, skeletal muscle isoform | 0.46 | 3–10 |
| 4333 | Myosin regulatory light chain 2, skeletal muscle isoform | 0.05[b] | 3–10 |
| 1678 | Peripherin | 1.25 | 4–7 |
| 1776 | Tropomyosin $\alpha$-chain (tropomyosin 1) | 0.61 | 4–7 |
| 4261 | Tropomyosin $\beta$-chain (tropomyosin 2) | 0.27 | 3–10 |
| 1914 | Tubulin $\alpha$-chain | 0.78 | 4–7 |
| 1870 | Tubulin $\alpha$-chain | 1.50 | 4–7 |
| 1908 | Tubulin $\beta$-chain | 0.75 | 4–7 |
| 2012 | Tubulin $\beta$-chain | 0.69 | 4–7 |
| **Signaling** | | | |
| 2621 | 14-3-3 protein $\beta/\alpha$ (PKC inhibitor protein) | 1.34 | 4–7 |
| 1774 | 14-3-3$\tau$ (14-3-3$\theta$) | 0.46 | 4–7 |
| 4347 | Acidic FGF (FGF-1) | 0.05[b] | 3–10 |
| 3931 | Astrocytic phosphoprotein PEA-15 | 1.50 | 3–10 |
| 1881 | Dihydropyrimidinase-related protein 2 (CRMP2) | 0.90 | 4–7 |
| 1681 | Guanine nucleotide-binding protein (transducin $\alpha$-chain) | 2.00 | 4–7 |
| 2164 | Guanine nucleotide-binding protein (transducin $\beta$-chain 2) | 20.00[2] | 4–7 |
| 4020 | Rho-GDP dissociation inhibitor 1$\alpha$ | 1.55 | 3–10 |
| 4521 | Rho-GDP dissociation inhibitor 1$\alpha$ | 20.00[b] | 3–10 |
| 1748 | Serine/threonine protein phosphatase 2A | 1.80 | 4–7 |

[a] Spots correspond to statistically significant ($p \leq 0.05$, one-way analysis of variance; normalization per gel as well as to the median of the three biological replicate gels and a call (present/absent) filter (two out of three biological replicates, WT and/or KO) were applied) regulated cytoskeletal and signaling proteins.

[b] Spots present only in KO or WT protein lysates were assigned the arbitrary values of 20 (20-fold increase; present only in the KO protein lysates) and 0.05 (20-fold decrease; present only in the WT protein lysates).

48 h and then treated for 1 h with increasing concentrations (5, 10, 20, and 40 $\mu$g/ml) of the S3 peptide or reverse-sequence control RV peptide.

*Retinal Ganglion Neuron Cultures*—Immortalized retinal ganglion neurons (RGC-5; provided by Dr. Krishnamoorthy (Department of Cell Biology and Genetics, University of Texas Health Science Center, Fort Worth, TX) were grown for 3 days in Dulbecco's modified Eagle's medium + GlutaMAX (Invitrogen), 10% fetal bovine serum, and 1% penicillin/streptomycin. Following trypsinization, cells were counted and plated on poly-L-lysine-coated coverslips (20 $\mu$g/ml) at a density of 10,000 cells/100 $\mu$l. Cells were grown overnight and then treated for 1 h with 20 $\mu$g/ml S3 peptide or reverse-sequence control RV peptide.

*Time-lapse Video Microscopy*—Dissociated DRG from adult Nogo-A KO and WT mice were cultured for 14 h in 2-well Lab-Tek chambered coverglass (Nalge Nunc International). Samples were then observed under a Leica wide-field IRBE microscope by phase contrast at 37 °C and 5% $CO_2$ with a ×100 oil immersion objective. Images were captured with a Hamamatsu camera using Openlab 3.1.7 software (Improvision). At least five KO as well as WT neurons were randomly chosen, and the largest growth cone of each of them was imaged. Six independent experiments were performed. For each growth cone, 60 images at intervals of 15 s were acquired for a total real time of 15 min of recordings. Movies were further processed using Openlab and QuickTime (Apple) (0.15 s/frame). Statistical data analysis was performed using Prism 4.0. For S3 and RV peptide treatments, after 13 h of culturing, KO and WT adult dissociated DRG were treated with 20 $\mu$g/ml peptide for 1 h and then imaged as described above with a ×40 oil immersion objective.

*Immunoblotting*—The spinal cords from eight adult Nogo-A KO as well as WT mice were processed for protein lysate as described for two-dimensional gel electrophoresis. Samples (30 $\mu$g/lane) were resolved on 7–14% NuPAGE (Invitrogen) and transferred onto polyvinylidene difluoride membranes, followed by blocking and overnight incubation

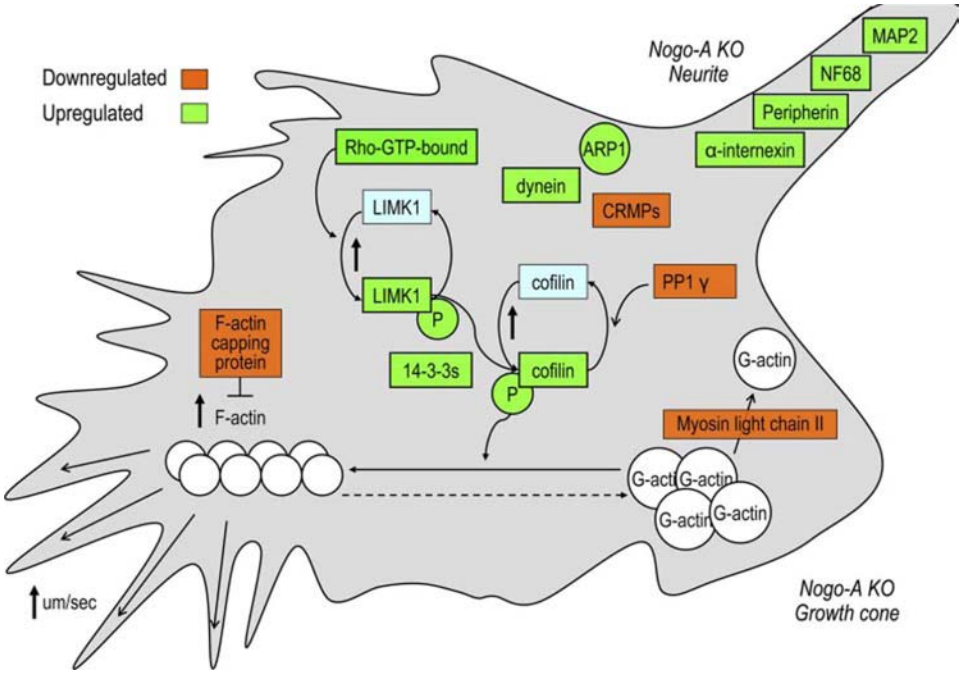


FIGURE 3. **Suggested molecular model for the observed changes in growth cone motility in Nogo-A KO neurons.** Up-regulation of phosphorylated active LIMK1 due to the up-regulation of Rho-GTPase signaling activity is translated into downstream phosphorylation and therefore deactivation of the actin-severing protein cofilin. This deactivation is further supported by the down-regulation of PP1, one of the players responsible for the turnover of phosphorylated cofilin into active cofilin, as well as by the up-regulation of 14-3-3 proteins, which can stabilize phosphorylated cofilin. Cofilin inactivation coupled to the down-regulation of actin polymerization-impeding factors, like F-actin-capping protein, allows the increase in actin polymerization required for the formation of new actin filopodia and for the extension of the growth cone. This process is further supported by the down-regulation of myosin II, which is responsible for the retrograde flow of G-actin. These changes could be further influenced by the down-regulation of CRMP2 and CRMP5, the signal of which is involved in growth cone collapse response. The enhancement of the neurite outgrowth machinery is supported by the regulation of specific neurofilaments, *e.g.* neurofilament-68, α-internexin, MAP2, and peripherin.

with primary antibodies at 4 °C. After washing, membranes were incubated with secondary antibodies. Proteins were detected using a chemiluminescent substrate (SuperSignal West Pico, Pierce). Images were captured with the Stella system (Agilent Technologies). Densitometry was performed with AIDA software (Raytest GmbH). Data analysis was performed using Prism 4.0.

*Immunocytochemistry*—Cells were fixed in 4% paraformaldehyde for 15 min at room temperature and permeabilized (0.1% Triton X-100 and 1× phosphate-buffered saline). After blocking, cells were incubated for double staining with primary antibodies, followed by incubation with the appropriate secondary antibody for 30 min and with 4′,6-diamidino-2-phenylindole. Activated Rho was detected by probing cells with the Rho-binding domain from the Rho-GTP-interacting protein rhotekin tagged with glutathione *S*-transferase. Antibodies against glutathione *S*-transferase were subsequently used. Preparations were mounted in Mowiol/1,4-diazabicyclo-[2.2.2]octane before examination under a conventional fluorescence microscope (Axio Scope 2 MOT Plus, Zeiss). Imaging was performed using an AxioVision system.

## RESULTS

*Profiling of Nogo-A KO Versus WT Unlesioned Adult Mouse Spinal Cord by Two-dimensional Gel Electrophoresis and ICAT*—We analyzed the spinal cords of C57BL/6 adult Nogo-A KO *versus* WT mice by two-dimensional gel electrophoresis (pH 4–7 and 3–10 isoelectrofocusing strips both used to increase the number of identified regulated spots) (Fig. 1 and supplemental Fig. 1) and ICAT (Fig. 2), followed by HPLC peptide separation and subsequent run and analysis through a liquid chromatography/tandem mass spectrometer. With two-dimensional gel electrophoresis, 93 regulated spots were identified, corresponding to 62 different known proteins/protein subunits. 16 of the identified proteins were represented in more than one regulated spot, pointing to a different post-translational modification state in Nogo-A KO *versus* WT tissue (Table 1). Up- and down-regulation were equally represented (51.6% up-regulated and 48.4% down-regulated spots). Assignment to functional categories on the basis of GeneOntology and literature mining showed that the highest number of regulated proteins or spots fell into the cytoskeleton category (17% and 33%, respectively). The other major functional categories significantly represented (% proteins and % spots) were neuroprotection (17% and 13%), metabolism (12% and 10%), and transport (7% and 6%) (Fig. 1). Only one regulated myelin protein was observed (myelin basic protein, 0.52-fold). The complete list of protein changes is shown in supplemental Table 1. The quantitative ICAT analysis allowed the identification of a high number of regulated proteins, in particular of hydrophobic membrane proteins, due to the avoidance of the loading/separation in a gel matrix. 407 proteins were identified with a ProteinProphet probability score of ≥0.9 (71.7%, ≥2 unique peptides) (Fig. 2*A* and supplemental Table 2) with a normal distribution of ~1.19 ± 0.02 (mean ratio) (Fig. 2*B*). All ratios have been normalized to this value, assuming a correct mean ratio of 1.000, to correct for possible errors in protein quantification. 219 proteins showed a -fold change ratio of between 0.5 and 2 in Nogo-A KO *versus* WT spinal cord. Proteins outside of this interval were normally distributed in terms of up-regulation (16.5%) and down-regulation (15.5%). 104 proteins showed statistically significant regulation according to adjusted ASAPRatio and S.E. (supplemental Table 2) and were categorized into functional categories using Panther Version 6.1 software and literature mining (Fig. 2*C*). The results reflected those observed with the two-dimensional gel electrophoresis approach: signaling (14%), metabolism (14%), transport (11%), cytoskeleton (9%), and neuroprotection (5%) were the major represented categories (Fig. 2*C*).

**TABLE 2**

**Differentially expressed cytoskeleton and signaling proteins in the spinal cords of Nogo-A KO versus WT mice by ICAT**

Proteins found regulated also by two-dimensional gel electrophoresis are shown in boldface. The applied threshold for protein probability score was $p \geq 0.9$.

| *p* | Description | Adjusted ratio | |
|---|---|---|---|
| | | Mean | S.D. |
| **Cytoskeleton** | | | |
| 1 | Transgelin-3 | 2.04 | 0.22 |
| 1 | Tetraspanin-2 | 0.34 | 0.11 |
| 1 | Splice isoform 2 of AP-2 complex subunit $\beta$1, splice isoform 1 of AP-2 complex subunit $\beta$1 | 0.19 | 0.04 |
| **1** | **Predicted: similar to cofilin-1 (cofilin, non-muscle isoform)** | **0.66** | **0.27** |
| 0.98 | Predicted: microtubule-associated protein (MAP2) | 2.05 | 0.62 |
| 1 | Microtubule-associated protein RP/EB family member 3 | 1.81 | 0.59 |
| 1 | Lap3 protein | 0.29 | 0.06 |
| **1** | ***In vitro*-fertilized egg cDNA, RIKEN full-length enriched library, clone 7420442C15, product $\gamma$-actin, cytoplasmic, full insert sequence; bone marrow macrophage cDNA, RIKEN full-length enriched library, clone I830072C08, product $\beta$-actin, cytoplasmic, full insert sequence; actin, cytoplasmic 1; actin, cytoplasmic 2** | **1.23** | **0.22** |
| 1 | Impact protein | 0.72 | 0.21 |
| 1 | F-actin-capping protein $\alpha_2$-subunit | 0.69 | 0.15 |
| 1 | Cytoplasmic dynein heavy chain, dynein heavy chain, cytosolic | 15.54 | 5.64 |
| 1 | Complexin-1 | 1.72 | 0.30 |
| 1 | AP-2 complex subunit $\alpha$2 | 1.57 | 0.43 |
| 1 | 117-kDa protein, ankyrin 2, brain | 0.35 | 0.06 |
| **Signaling** | | | |
| **1** | **Splice isoform 2 of 14-3-3$\theta$, splice isoform 1 of 14-3-3$\theta$** | **1.70** | **0.55** |
| 1 | **Rho-related GTP-binding protein RhoB precursor** | 0.34 | 0.12 |
| 1 | **Ras-related protein Rab-3D** | 0.22 | 0.06 |
| 0.99 | Predicted: similar to 14-3-3$\eta$,14-3-3$\eta$ | 1.48 | 0.30 |
| 0.98 | Predicted: hypothetical protein LOC75471; GTP-binding nuclear protein Ran, testis-specific isoform; GTP-binding nuclear protein Ran | 0.50 | 0.13 |
| 1 | Mammary gland RCB-0527 Jyg-MC(B) cDNA, RIKEN full-length enriched library, clone G930005L08, product Ras-related C3 botulinum substrate 1, full insert sequence | 0.68 | 0.23 |
| **1** | **Guanine nucleotide-binding protein $G_o$ $\alpha$-subunit 2; guanine nucleotide-binding protein $G_o$ $\alpha$-subunit 1** | **0.69** | **0.19** |
| **1** | **Guanine nucleotide-binding protein $G_I/G_S/G_T$ $\gamma$-subunit 2** | **0.71** | **0.09** |
| 1 | Dihydropyrimidinase-related protein, 5.62 kDa (CRMP5) | 0.72 | 0.24 |
| 1 | 14-3-3$\gamma$ | 1.28 | 0.25 |

*Molecular Reorganization of the Neurite Outgrowth Machinery in the Intact Adult Nervous System of Nogo-A KO Mice*—The category "cytoskeleton" was the one mainly represented in the changes found in our proteomic approach. With two-dimensional gel electrophoresis, we observed a higher number of regulated spots (33%) than of proteins (17%) (Fig. 1), indicating an important role of post-translational modifications in the regulation of the cytoskeleton in response to Nogo-A ablation. In addition to actin and tubulin isoforms, many of the differentially expressed proteins play an important role in actin and tubulin cytoskeleton remodeling (Fig. 3 and Table 1). Particularly interesting is cofilin, previously suggested to be downstream of Nogo-A/Nogo-66 receptor signaling (31); it showed two regulated spots, 0.79 (−1.27)- and 1.70-fold, respectively (Table 1), pointing to a diverse post-translational modification state of this protein. Cofilin phosphorylation state, regulated by LIMK1, is known to affect actin cytoskeleton dynamics, growth cone motility, and neurite outgrowth (Fig. 3). The changes in actin-binding proteins (myosin, tropomyosin) as well as actin itself (Table 1) suggested that the actin cytoskeleton was directly affected. In addition, neuronal intermediate filaments, *e.g.* peripherin, neurofilament-68, and $\alpha$-internexin, which are highly expressed during development and in early neurite formation, were also regulated, suggesting the whole neuronal cytoskeleton to be affected by the lack of Nogo-A (Table 1). This conclusion was supported by the high number of spots (12%) and proteins (15%) falling into the category of signaling molecules (Fig. 1), the majority of which belonged to pathways responsible for cytoskeleton rearrangements and neurite outgrowth control. Examples are the 14-3-3 family of proteins (known to interact with cofilin as well as with its major regulator, LIMK1) and Rho-GDP dissociation inhibitor 1 (a key regulatory molecule of Rho-GTPase signaling pathways (Table 1), which can, upstream of LIMK1, affect its phosphorylation and therefore activity state).

We observed also the down-regulation of CRMP2, a protein playing a role in growth cone collapse (Table 1). The comparison and integration of the ICAT data with the two-dimensional gel electrophoresis data permitted us to strengthen our observation of an important response at the level of the neuronal cytoskeleton and signaling machinery (Figs. 2 and 3 and Table 2). Cytoskeletal proteins known to affect actin polymerization (F-actin-capping protein, 0.69 ± 0.15), neurite outgrowth (microtubule-associated protein RP/EB3, 1.81 ± 0.59; MAP2, 2.05 ± 0.62), or microtubule-dependent transport (dynein, 15.54 ± 5.64) were shown to be regulated in a direction pointing to growth enhancement: down-regulation of actin-severing proteins and up-regulation of motor as well as microtubular proteins. The total level of cofilin presented a slight down-regulation (0.66 ± 0.27) (Table 2). This technique allowed only the quantification of the total level of relative cofilin expression but did not permit the discrimination between phosphorylated and unphosphorylated forms. Among the other regulated signaling proteins emerged again the 14-3-3 proteins (14-3-3$\theta$, 1.7 ± 0.55; 14-3-3$\eta$, 1.48 ± 0.30; 14-3-3$\gamma$, 1.28 ± 0.25) as well as a member of the CRMP protein family (dihydropyrimidinase-related protein 5, 0.72 ± 0.25). The Rho-GTPase signaling pathway was also affected (Rho-related GTP-binding protein

RhoB precursor, 0.34 ± 0.12; Ras-related C3 botulinum substrate 1 (Rac1), 0.63 ± 0.23) (Table 2). All of the observed regulated pathways are known to affect cytoskeleton dynamics and in particular point to the Rho-GTPase signaling pathway, which can affect the phosphorylation state of LIMK1, which can in turn phosphorylate and inactivate cofilin (32). As shown below, we observed an increase in cofilin phosphorylation. Therefore, the Rho-GTPase/LIMK1/cofilin signaling pathway is clearly a candidate in the regulation of neuronal cytoskeletal proteins in the absence of Nogo-A signaling in the intact adult CNS.

*Modulation of the Rho-GTP/LIMK1/Cofilin Pathway in the Adult CNS and in Dissociated DRG Neurons from Adult Nogo-A KO Mice*—Cofilin is an actin-severing protein inactivated through phosphorylation. It can directly affect actin polymerization rate, actin filopodial formation, and growth cone motility (32, 33) and, as shown recently, neurite outgrowth (34). The activation state of LIMK1 has been shown to play a key role in regulating the phosphorylation state of cofilin (32). We tested the levels of total and phosphorylated cofilin and LIMK1 in the spinal cords of unlesioned adult Nogo-A KO *versus* WT mice by Western blotting (Fig. 4, *A* and *B*). Densitometry confirmed increased levels of phosphorylated, and therefore inactive, cofilin in Nogo-A KO mice. It also showed increased levels of phosphorylated, and therefore active, LIMK1. No change was detected in total protein levels. These data support a role of the LIMK1 activation state in the regulation of cofilin phosphorylation and inactivation (Fig. 4, *A* and *B*) in the intact spinal cords of adult Nogo-A KO mice.

To clarify if these changes could be ongoing in Nogo-A KO adult neurons, as a recent study from Endo *et al.* (34) has shown that LIMK1 regulates actin filament assembly at the tips of the growth cones of chick DRG neurons and as DRG neurons are one of the few populations of adult neurons with axons in the CNS that can be maintained in culture, we analyzed by immunocytochemistry the levels of phosphorylated and total LIMK1 in the growth cones of Nogo-A KO and WT adult dissociated DRG neurons after 14 h in culture (Fig. 5*A*). The results show that the levels of phosphorylated LIMK1 were increased in the growth cones (KO, 1.46 ± 0.16; WT, 1.0 ± 0.08) of Nogo-A KO compared with WT neurons (Fig. 5*A*). However, no change could be detected for the total level of expression of LIMK1 (KO, 1.158 ± 0.06; WT, 1.0 ± 0.06) (Fig. 5*A*).

LIMK1 phosphorylation is regulated through activation of ROCK by Rho-GTP and of PAK1 by Rac and Cdc42. Interestingly, our proteomic data already pointed to a potential regulation of Rho-GTPases in the intact nervous system of Nogo-A KO mice. Up to now, Nogo-A has been known to affect only RhoA activation. Therefore, we tested the level of Rho-GTP *in vitro* in Nogo-A KO and WT adult dissociated DRG and observed up-regulation of activated Rho in the growth cones of Nogo-A KO neurons (KO, 1.56 ± 0.1; WT, 1.0 ± 0.04), pointing to its potential involvement in the increase of LIMK1 phosphorylation (Fig. 5*B*).

*Neurons from Adult Nogo-A KO Mice Show Altered Growth Cone Morphology and Increased Growth Cone Motility*—The LIMK1/cofilin pathway, shown recently to directly affect neurite outgrowth and actin filopodial formation at the tip of the growth cone in chicken DRG (34), as well as the observed modulation of other signaling molecules participating in this pathway and/or known to affect cytoskeletal dynamics (14-3-3 and CRMP proteins and Rho-GTPases) and the changed expression levels of several additional cytoskeleton and cytoskeleton-binding proteins such as dynein and myosin II, which have been suggested to increase neurite and growth cone motility when up-regulated (35–37), could influence the morphology and dynamic aspects of the neuronal cytoskeleton of Nogo-A KO adult neurons (Fig. 3). Nogo-A KO adult dissociated DRG neurons plated onto a polylysine/laminin substrate and kept 14 h in culture did not show significant differences in the number of emitted neurites or in branching points compared with WT DRG neurons (supplemental Fig. 2). However, they showed a clear shift toward larger growth cones (≥100 $\mu m^2$) and a corresponding reduction in smaller growth cones (≤50 $\mu m^2$) compared with WT DRG neurons (Fig. 6*A*). Taking the overall morphology and distribution of F-actin and microtubules into account, we categorized the growth cones into dystrophic (38), normal, and enlarged (Fig. 6*A*). The percentage of neurons presenting enlarged growth cones was significantly higher in Nogo-A KO dissociated DRG cultures (KO, 35 ± 6.60%; WT, 13.30 ± 6.72%) (Fig. 6*A*). A more accurate analysis of the

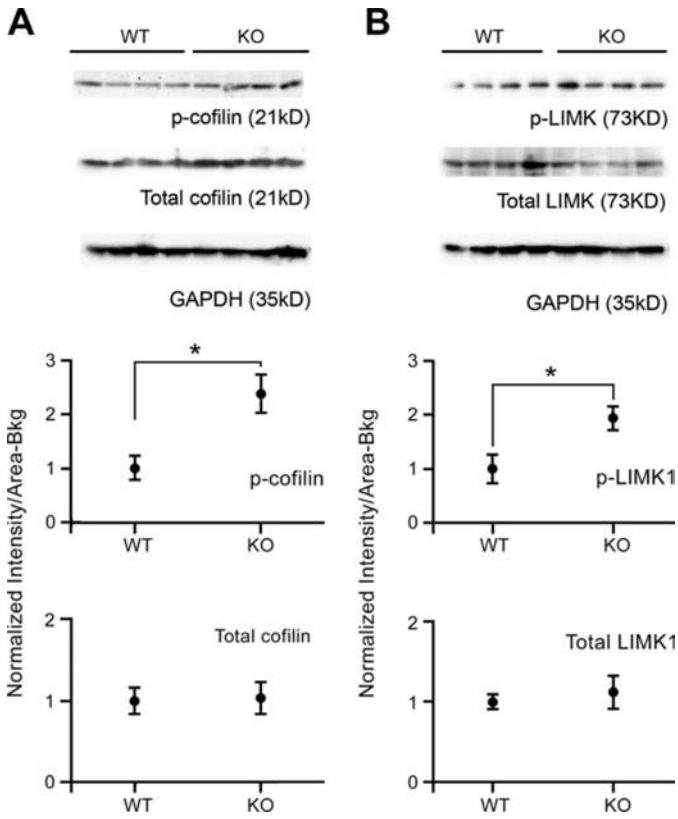


FIGURE 4. **Modulation of the LIMK1/cofilin pathway in the spinal cords of adult Nogo-A KO mice.** *A* and *B*, representative images of Western blots and corresponding densitometric quantification reporting the level of expression of phosphorylated cofilin (*p-cofilin*) and total cofilin (*A*) and phosphorylated LIMK1 (*p-LIMK*) and total LIMK1 (*B*) in spinal cord lysates from WT and Nogo-A KO mice. Results show increased phosphorylation of cofilin and of the cofilin regulator LIMK1 in the spinal cords of unlesioned adult Nogo-A KO mice. Protein levels have been normalized to the expression levels of glyceraldehyde-3-phosphate dehydrogenase (*GAPDH*) ($n = 8$; *, $p < 0.05$, Mann-Whitney test). *Bkg*, background.

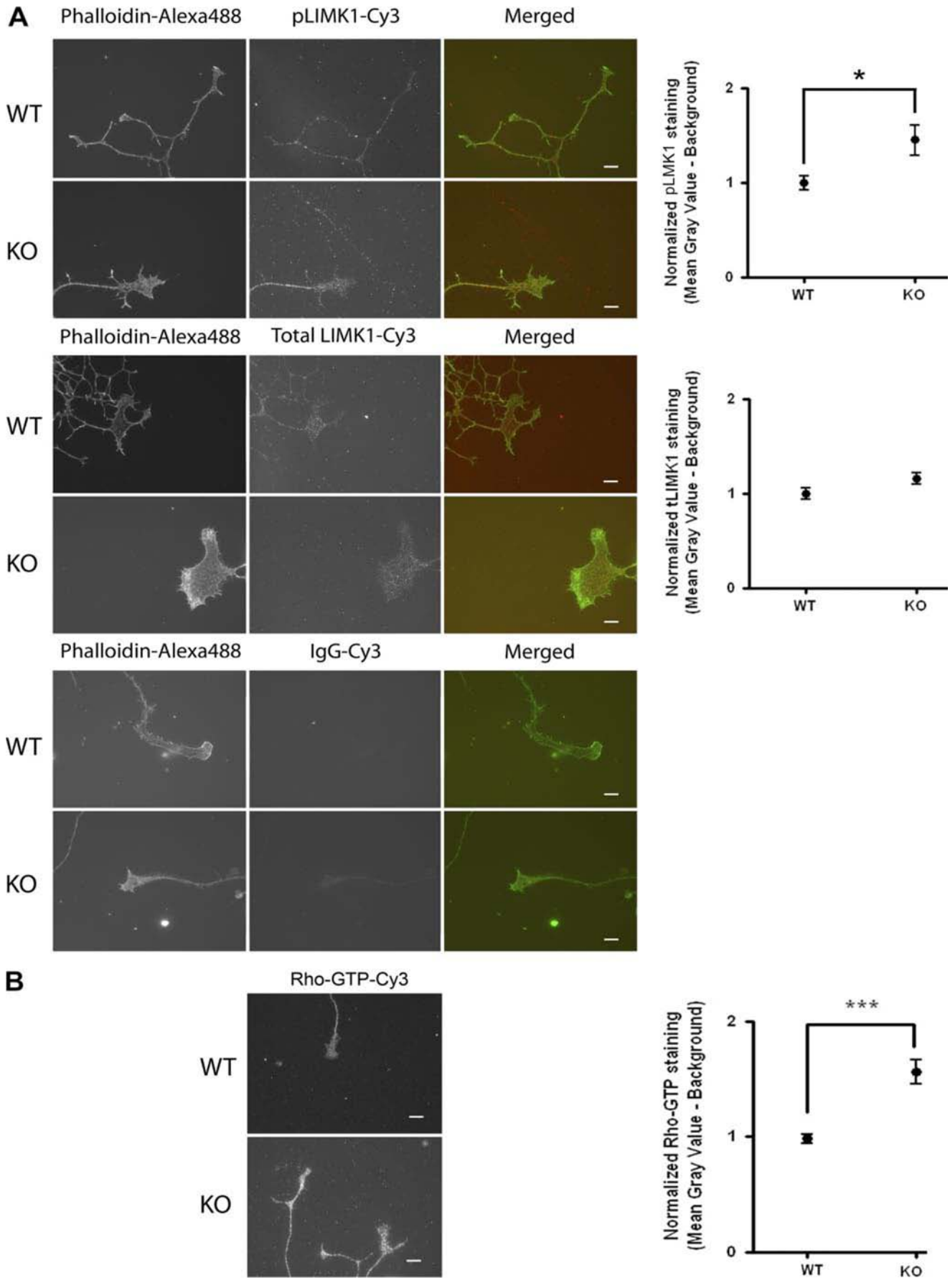
A
Phalloidin-Alexa488
pLIMK1-Cy3
Merged
WT
KO
Normalized pLMK1 staining
(Mean Gray Value - Background)
*
2
1
0
WT
KO
Phalloidin-Alexa488
Total LIMK1-Cy3
Merged
WT
KO
Normalized tLIMK1 staining
(Mean Gray Value - Background)
2
1
0
WT
KO
Phalloidin-Alexa488
IgG-Cy3
Merged
WT
KO
B
Rho-GTP-Cy3
WT
KO
Normalized Rho-GTP staining
(Mean Gray Value - Background)
***
2
1
0
WT
KO

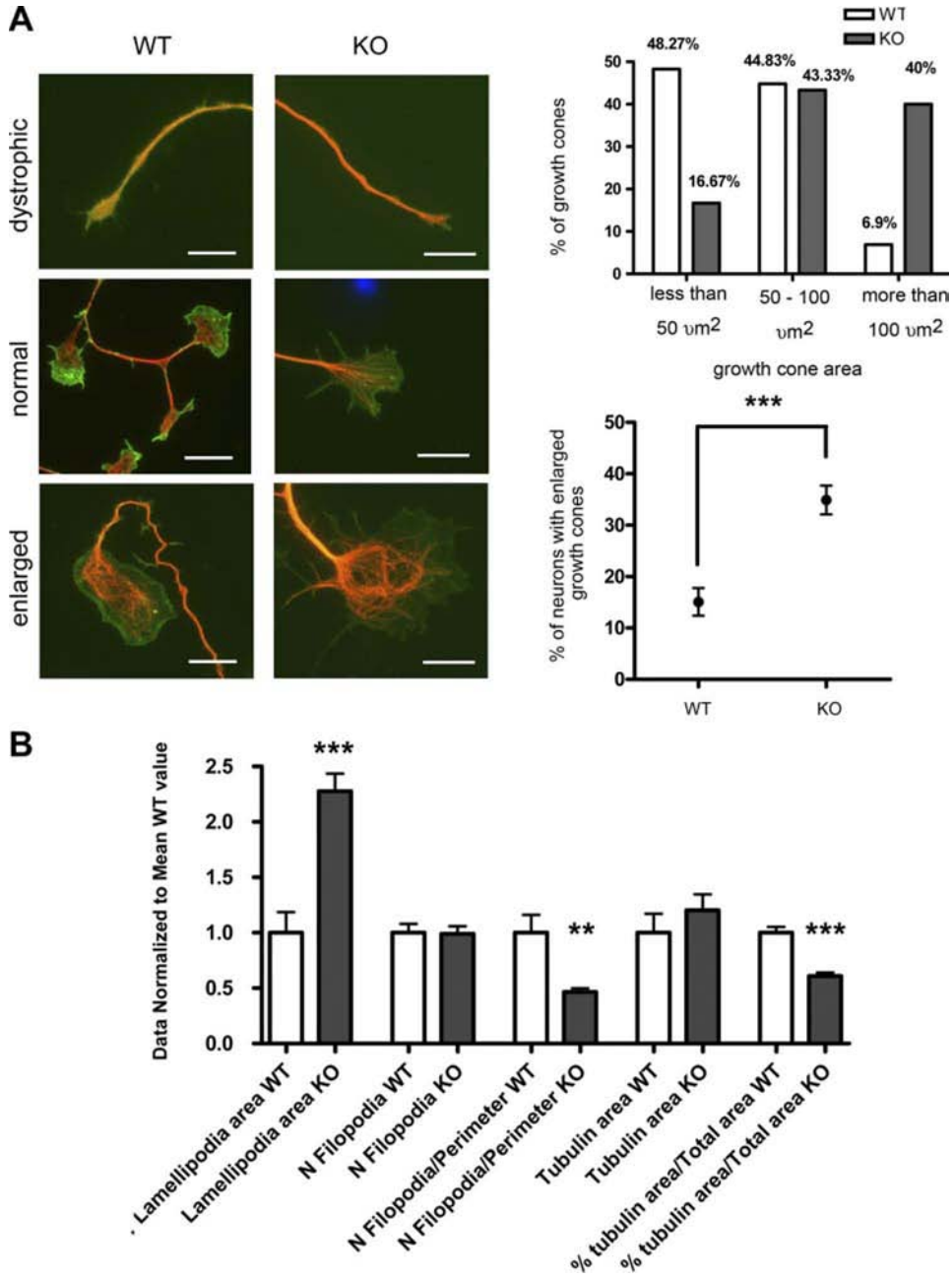


FIGURE 6. **Neurons from adult Nogo-A KO mice show altered growth cone morphology and motility.** *A*, representative examples of dystrophic (38), normal, and enlarged growth cones as observed in WT and Nogo-A KO adult dissociated DRG neurons labeled for microtubules (Cy3-anti-$\beta$-tubulin (*red*)) and F-actin (Alexa 488-phalloidin (*green*)). Shown is the distribution of WT and KO growth cones according to their areas ($<$50, 50–100, and $\geq$100 $\mu m^2$). The percentage of WT and Nogo-A KO neurons showing enlarged growth cones was calculated for the total number of evaluated neurons in three independent experiments (***, $p < 0.0001$, Mann-Whitney test). *Error bars* represent S.E. *B*, analysis of lamellipodia and filopodia in growth cones of Nogo-A KO and WT adult dissociated DRG neurons. Data have been normalized to the mean of the WT values ($n = 50$ per group, two independent experiments; **, $p < 0.001$, Mann-Whitney test; ***, $p < 0.0001$).

growth cones has shown that the increase in growth cone area is specifically due to an increase in the area covered by actin-containing lamellipodia (KO, 2.28 $\pm$ 0.16; WT, 1.0 $\pm$ 0.19), whereas no difference could be observed in the tubulin-containing core area (KO, 1.2 $\pm$ 0.14; WT, 1.0 $\pm$ 0.17). These data are reflected in the measured decrease in the percentage of the tubulin-containing core area over the total area of Nogo-A KO *versus* WT growth cones (KO, 0.61 $\pm$ 0.03; WT, 1.0 $\pm$ 0.05). To test whether more F-actin polymerization could result in an increase in both lamellipodia and filopodia, we counted the number of filopodia per growth cone. No significant change was present in the total filopodial number (KO, 0.99 $\pm$ 0.07; WT, 1.0 $\pm$ 0.08). However, due to the larger lamellipodial area, a decrease in the number of filopodia in relation to the perimeter of the growth cone was observed (KO, 0.47 $\pm$ 0.03; WT, 1.0 $\pm$ 0.16) (Fig. 6*B*).

To check the specificity of the observed morphological changes, we performed an additional set of experiments in which we specifically and acutely blocked Nogo-A, present on the cell membranes of adult DRG (24), in culture by adding anti-Nogo-A antibodies (11C7) (Fig. 7, *A* and *B*) to dissociated DRG from WT mice. An IgG antibody was applied as a control, and Nogo-A KO adult dissociated DRG were treated as well with both antibody 11C7 or IgG as an additional control (Fig. 7*B*). The specific neutralization of Nogo-A reproduced the neuronal phenotype observed in Nogo-A KO neurons, showing an increase in the percentage of neurons with enlarged growth cones (Fig. 7*B*), suggesting that the observed phenotype is specifically due to the lack of

FIGURE 5. **Regulation of Rho-GTP, LIMK1 and phosphorylated LIMK1 at the growth cones of Nogo-A KO neurons.** *A*, representative immunofluorescence images showing Cy3-phosphorylated LIMK1 (*pLIMK1*) and Cy3-total LIMK1 staining in growth cones of WT and Nogo-A KO adult dissociated DRG neurons cultured for 14 h and densitometric quantification of staining intensity. For each growth cone, F-actin staining with Alexa 488-phalloidin and merged images are also shown. Results show increased phosphorylation of LIMK1 but no increase in total LIMK1 (*tLIMK1*). The data have been normalized to the mean of the WT values ($n = 20$ per group; *, $p < 0.05$, Mann-Whitney test). *Scale bars* = 10 $\mu$m. *Error bars* represent S.E. Cy3-IgG (control) did not show any specific staining. *B*, representative immunofluorescence images showing Cy3-Rho-GTP staining (rhotekin) in growth cones of WT and Nogo-A KO adult dissociated DRG neurons cultured for 14 h and densitometric quantification of staining intensity. Results show an increase in Rho-GTP in Nogo-A KO growth cones. The data have been normalized to the mean of the WT values ($n = 20$ per group; ***, $p < 0.0001$, Mann-Whitney test). *Scale bars* = 10 $\mu$m.

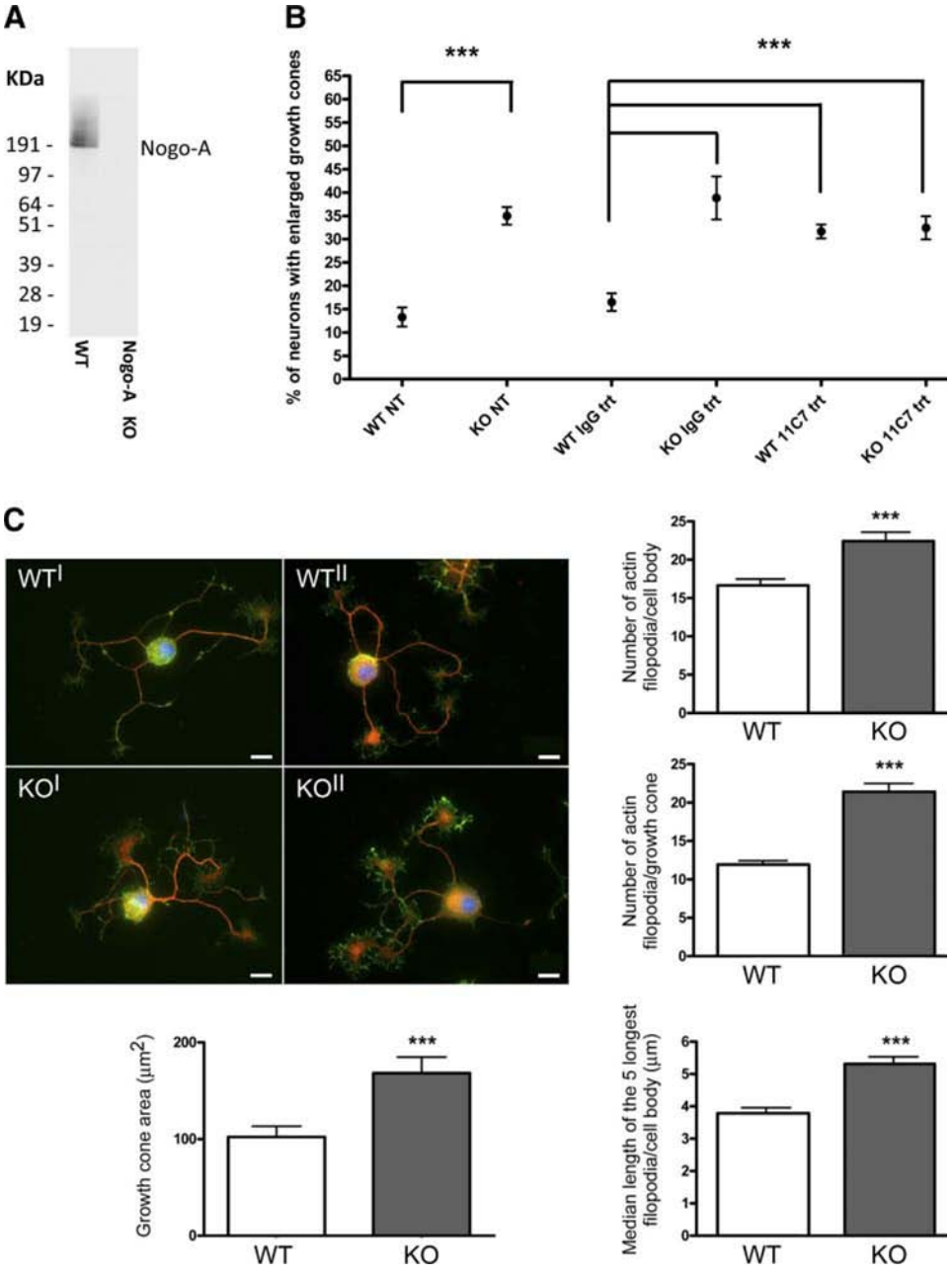


FIGURE 7. **Antibody-mediated neutralization and genetic ablation of neuronal Nogo-A affect growth cone morphology.** *A*, Western blots showing the specific detection of one single band corresponding to the expected molecular weight for Nogo-A with anti-Nogo-A mouse monoclonal antibody 11C7 in spinal cord lysates from WT and Nogo-A KO mice. *B*, percentage of WT and Nogo-A KO neurons showing enlarged growth cones, with WT non-treated (*WT NT*) and WT IgG (*WT IgG trt*) as control treatments. The percentage was calculated for the total number of evaluated neurons (neurons per experiment and condition ≥ 20) in three independent experiments ($n = 3$; ***, $p < 0.0001$, Mann-Whitney test). *Error bars* represent S.E. *C*, genetic ablation of Nogo-A influences growth cone morphology also of P0 DRG neurons. Shown are representative images of Nogo-A KO and WT newborn dissociated DRG neurons after 6 h in culture. Immunofluorescence labeling was performed with Cy3-anti-β-tubulin (*red*) and Alexa 488-phalloidin (*green*)). *Scale bars* = 10 μm. The area of Nogo-A KO and WT growth cones was quantified (***, $p < 0.0001$, Mann-Whitney test). *Error bars* represent S.E.

neuronal Nogo-A and not to additional compensating molecules, *e.g.* Nogo-B.

*Neuronal Nogo-A Influences Growth Cone Morphology Also in Newborn DRG Neurons*—To further understand whether the lack of Nogo-A signaling affects the growth cone machinery only of Nogo-A KO adult neurons or also during development, when Nogo-A expression is strictly neuronal, we dissociated DRG neurons from Nogo-A KO and WT newborn (P0) mice (Fig. 7*C*). As in adult neurons, no significant difference was detected in the number of branch points (KO, 8.26 ± 0.64; WT, 7.2 ± 0.45) or in the number of neurites per cell body (KO, 3.82 ± 0.18; WT, 3.53 ± 0.20) (data not shown). However, we were able to observe a substantial enlargement in the growth cone area of Nogo-A KO neurons (KO, 168.2 ± 16.71; WT, 102.30 ± 10.94) (Fig. 7*C*) as well as a major increase in the number of actin filopodia emitted from both the growth cone (KO, 21.41 ± 1.07; WT, 11.93 ± 0.51) and the cell body (KO, 22.43 ± 1.17; WT, 16.65 ± 8.61) (Fig. 7*C*). Furthermore, these filopodia were significantly longer (KO, 5.31 ± 0.22; WT, 3.79 ± 0.17) (Fig. 7*C*). These data further support a role of neuronal Nogo-A in actin cytoskeleton remodeling.

*Increased Growth Cone Motility in Nogo-A KO Adult Dissociated DRG Neurons*—To observe whether the changes at the morphological level shown in growth cones of Nogo-A KO neurons could also cause a functional modification in growth cone motility, we used time-lapse microscopy (supplemental Videos 1 and 2). As expected from the previous results, we found a clear increase in the mean area of growth cones of Nogo-A KO DRG neurons (initial area, 96.6 ± 9.9 $\mu m^2$; final area, 105.5 ± 10.6 $\mu m^2$ over a 15-min observation period) compared with WT DRG neurons (initial area, 54.6 ± 5.4 $\mu m^2$; final area, 61.1 ± 5.3 $\mu m^2$) (Fig. 8*A*). Furthermore, in 15 min, Nogo-A KO growth cones covered double the distance covered by WT growth cones (KO, 8.9 ± 0.9 μm; WT, 4.3 ± 0.7 μm), showing a strong increase in growth speed (Fig. 8*B*). Nogo-A KO growth cones showed higher minimum speed (KO, 0.16 μm/min; WT, 0.00 μm/min) as well as higher maximum speed (KO, 1.38 μm/min; WT, 0.94 μm/min). This increase was not due to a continuous enlargement over time in the area of Nogo-A KO growth cones or a restriction of WT ones, as the initial and final areas for each genotype were not statistically different (Fig. 8*A*). To test whether the observed speed difference was a secondary effect caused by different turning behavior of KO compared with WT growth cones, the rotation angle was measured, but no significant difference was observed (supplemental Fig. 3). If

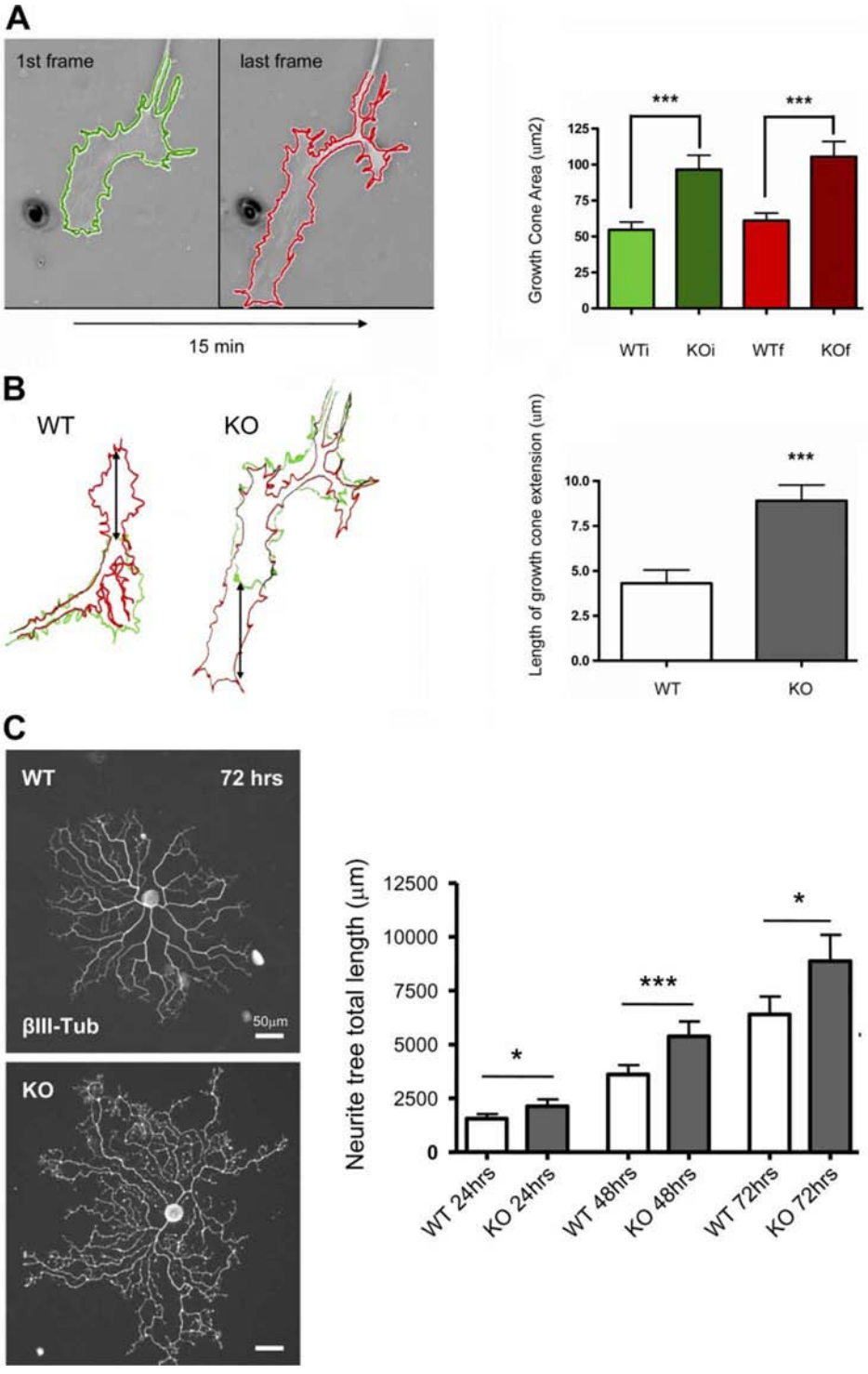


FIGURE 8. **Increased neurite outgrowth of Nogo-A KO dissociated DRG neurons.** *A*, following 13 h in culture, growth cones were filmed over 15 min. The first ($t = 0$ min) and last ($t = 15$ min) frames of each movie for both Nogo-A KO and WT growth cones have been traced with separate colors (first, *green*; last, *red*). Growth cone areas are shown in the corresponding *bar graph* (***, $p < 0.0001$, Mann-Whitney test). *Error bars* represent S.E. of six independent experiments. The initial and final tracings have been overlapped for further analysis. *B*, the *arrows* show the measured length of growth cone extension during the 15 min of recording. The mean lengths of growth cone extension are shown in the *bar graph* (***, $p < 0.0001$, Mann-Whitney test). *Error bars* represent S.E. *C*, shown are representative images of WT and Nogo-A KO adult dissociated DRG neurons at 3 days *in vitro* and immunofluorescently labeled with Cy3-anti-$\beta$-tubulin III (*βIII-Tub*). *Scale bars* = 50 $\mu$m. The total length of the neurite tree was measured by Metamorph software after 1–3 days *in vitro* in culture (*, $p < 0.05$, *t* test; ***, $p < 0.0001$). *Error bars* represent S.E.

Nogo-A KO growth cones advance more rapidly, longer neurites could be expected. We measured the total length of the neuritic tree of WT and Nogo-A KO adult dissociated DRG neurons after 1–3 days *in vitro*. The increase in growth cone area and speed did translate into a significant increase in the overall size of the neuronal tree (Fig. 8*C*).

*Inhibition of LIMK1 Activity Decreases Growth Cone Motility in Nogo-A KO Adult Dissociated DRG Neurons*—Endo *et al.* (34) recently found that a cell-permeable peptide containing the N-terminal sequence of cofilin and therefore its $Ser^3$ phosphorylation site (the S3 peptide) inhibits LIMK1 activity and reduces phosphorylated cofilin levels in the growth cones of chick DRG neurons. We confirmed that the S3 peptide, but not the reverse-sequence control RV peptide, can decrease cofilin phosphorylation and F-actin *in vitro* in native COS-7 cells (supplemental Fig. 4), NGF-primed PC12 cells, and retinal ganglion neurons (Fig. 9). To test whether the activity of LIMK1 could be directly responsible for the increased growth cone motility observed in Nogo-A KO adult DRG neurons, we inhibited LIMK1 in Nogo-A KO as well as WT dissociated DRG neurons. Time-lapse video analysis of S3 peptide-treated KO cultures showed clearly reduced growth cone motility compared with the control RV peptide-treated Nogo-A KO cells: KO S3 peptide-treated growth cones grew 6.93 $\pm$ 0.93 $\mu$m in 15 min, and KO RV peptide-treated growth cones grew 10.45 $\pm$ 0.88 $\mu$m in 15 min (Fig. 10*A*). The inhibition of LIMK1 in WT dissociated DRG neuronal cultures with the S3 peptide did not produce a significant decrease in growth cone motility compared with the control RV peptide: WT S3 peptide-treated growth cones grew 5.56 $\pm$ 0.63 in 15 min, and WT RV peptide-treated growth cones grew 5.59 $\pm$ 0.79 in 15 min (Fig. 10*B*). The inhibition of LIMK1 thus reversed almost completely the KO phenotype to the levels of

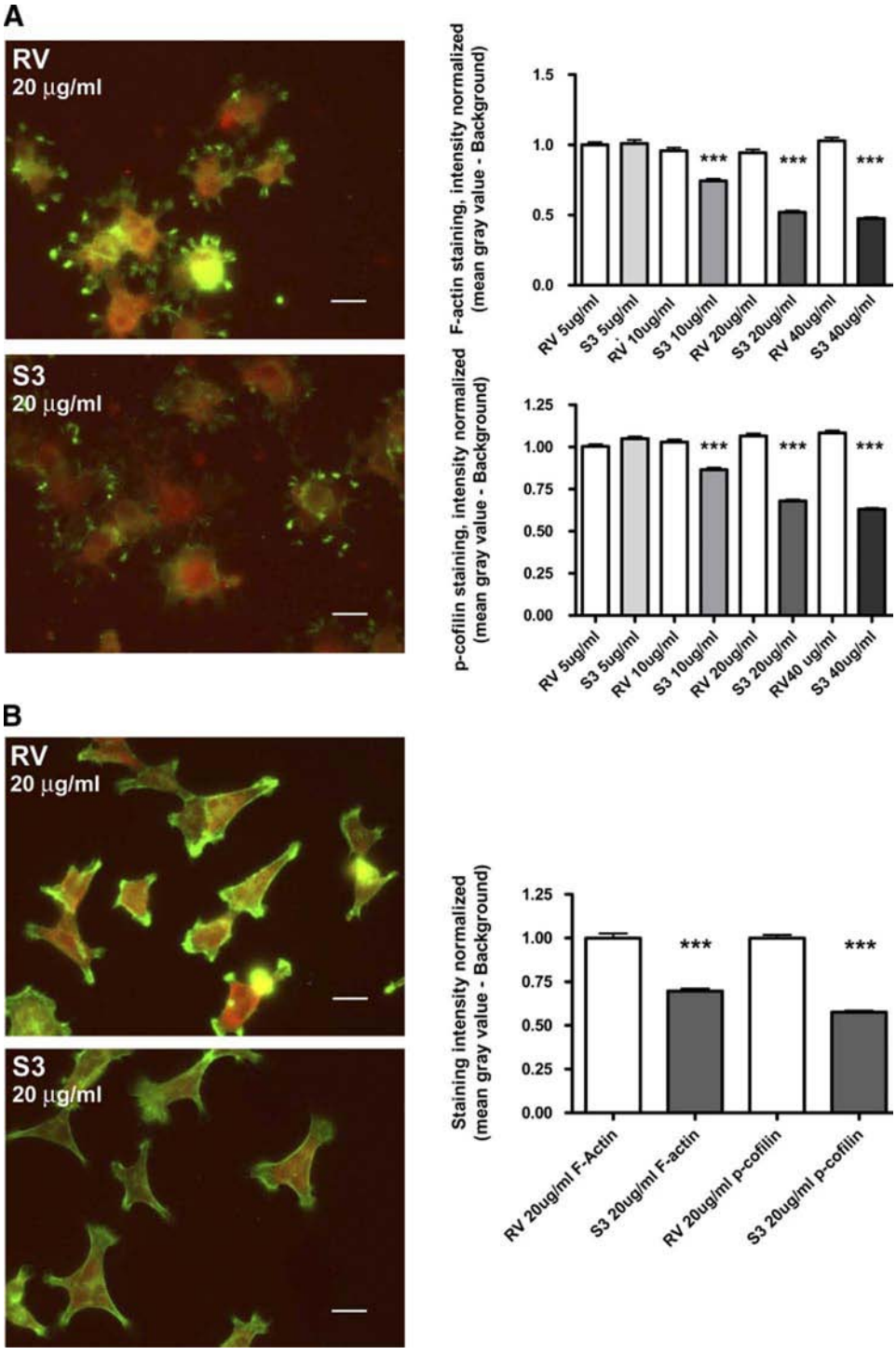


FIGURE 9. **S3 peptide treatment reduces phosphorylated cofilin and F-actin immunostaining in NGF-differentiated PC12 cells and retinal ganglion neurons.** *A*, representative immunofluorescence images of PC12 cells differentiated via NGF and treated for 1 h with 20 $\mu$g/ml S3 peptide or reverse-sequence control RV peptide. Immunofluorescence labeling was performed with Alexa 488-phalloidin (*green*) and Cy3-phosphorylated cofilin (*p-cofilin*; *red*). *Scale bars* = 20 $\mu$m. Quantification was performed by densitometry of phosphorylated cofilin and F-actin staining intensity following treatment with increasing concentrations (5, 10, 20, and 40 $\mu$g/ml) of the S3 peptide or reverse-sequence control RV peptide. The data have been normalized to the mean of the RV peptide-treated PC12 cell values ($n = 20$ per group, three independent experiments; ***, $p < 0.0001$, Mann-Whitney test). *Error bars* represent S.E. *B*, representative immunofluorescence images of retinal ganglion neurons treated for 1 h with 20 $\mu$g/ml S3 peptide or reverse-sequence control RV peptide. Immunofluorescence labeling was performed with Alexa 488-phalloidin (*green*) and Cy3-phosphorylated cofilin (*red*). *Scale bars* = 20 $\mu$m. Quantification was carried out by densitometry of phosphorylated cofilin and F-actin staining intensity following treatment with 20 $\mu$g/ml S3 peptide or reverse-sequence control RV peptide. The data have been normalized to the mean of the RV peptide-treated cell values ($n = 20$ per group, three independent experiments; ***, $p < 0.0001$, Mann-Whitney test). *Error bars* represent S.E.

growth cone extension length observed for WT neurons, indicating a role of the LIMK1/cofilin pathway in the observed phenotype.

## DISCUSSION

*Molecular Reorganization of the Neurite Outgrowth Machinery in the Intact Adult Nervous System of Nogo-A KO Mice*—Nogo-A KO mice have been extensively studied as a regeneration model following a CNS lesion (12–15), but the possible functions of Nogo-A in the intact CNS are still rather unclear. Therefore, in this study, we addressed this question using a double proteomic approach to investigate the molecular changes in the adult intact nervous system of Nogo-A KO mice. In line with previous reports of enhanced sprouting and fiber growth following antibody-mediated Nogo neutralization in the unlesioned rat adult CNS (25, 26), in our study, a reorganization and enhancement of the Nogo-A KO neuronal growth machinery at both the molecular and morphological levels could be observed.

We found that a large proportion of differentially expressed proteins in the Nogo-A KO intact adult nervous system are components of the cytoskeleton, cytoskeleton-binding proteins, signaling molecules involved in cytoskeleton remodeling and growth, early neurite growth markers, and axonal transport constituents. Numerous proteins that are known to play an important role in actin and tubulin cytoskeleton remodeling (*e.g.* F-actin-binding protein, dynein, myosin, and tropomyosin) were found to be regulated in a direction pointing to growth enhancement: down-regulation of actin-severing proteins and up-regulation of motor as well as structural proteins. The regulation of many neuron-specific cytoskeletal proteins, in particular neurofilament-68, peripherin, and $\alpha$-internexin, which are highly expressed during development and in early neurite formation, as well as of other neu-

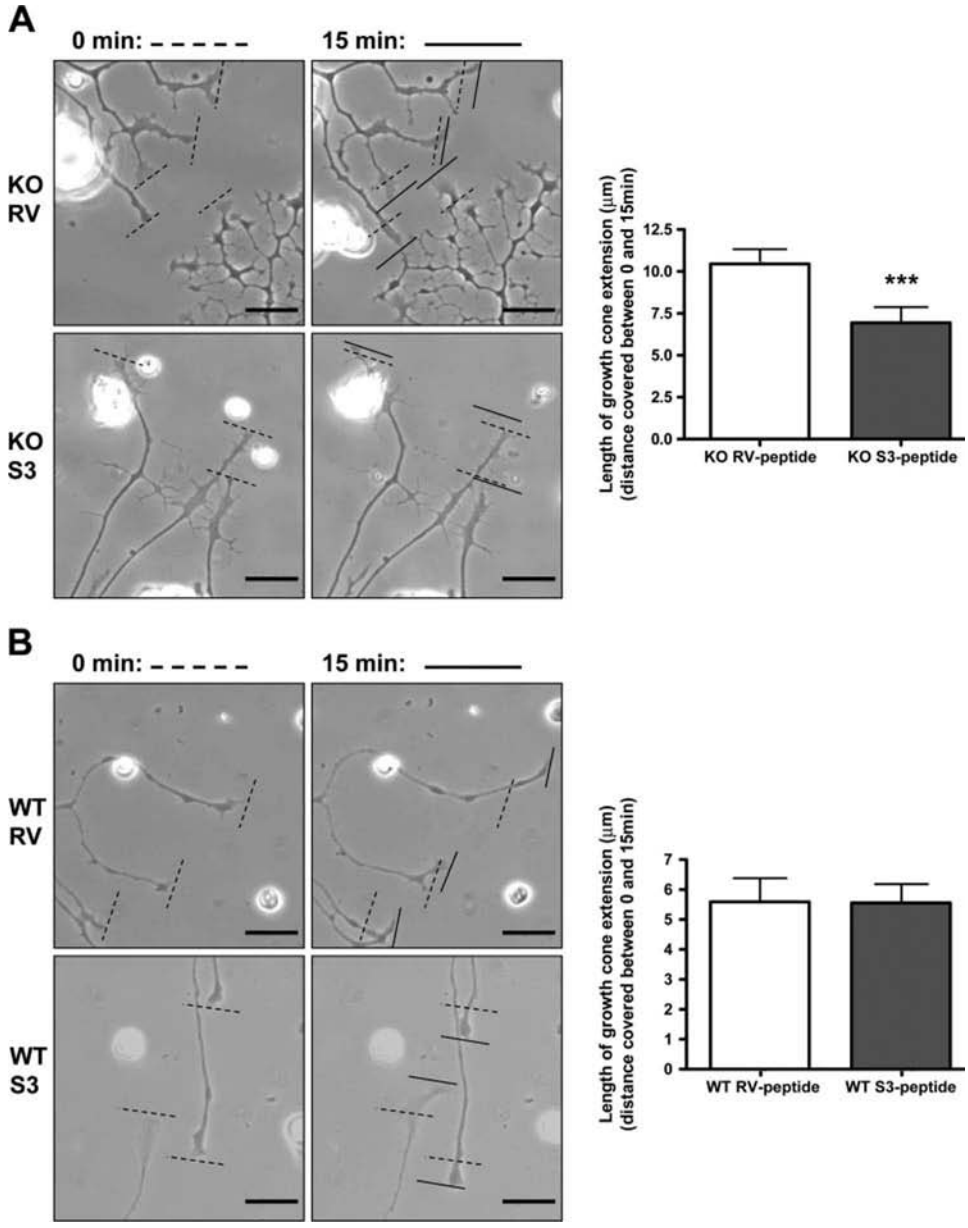


FIGURE 10. **Inhibition of LIMK1 activity decreases growth cone motility in Nogo-A KO adult dissociated DRG neurons.** *A* and *B*, dissociated DRG neurons from adult Nogo-A KO and WT mice, respectively, were grown for 13 h on a polylysine and laminin substrate. Cultures were treated for 1 h with 20 $\mu$g/ml S3 or RV peptide, and growth cones were then filmed over 15 min. Representative images of the first ($t = 0$ min) and last ($t = 15$ min) frames for S3 and RV peptide-treated cultures are shown. *Dashed lines* show the growth cone position at time point 0, and *solid lines* show the growth cone position after 15 min of imaging. *Scale bars* = 20 $\mu$m. The mean lengths of growth cone extension, corresponding to the distance between the *dotted* and *solid lines*, are shown in the *bar graphs* (quantified growth cones, $n \geq 30$, six independent experiments; ***, $p < 0.0001$, Mann-Whitney test). *Error* bars represent S.E.

ronal markers, such as MAP2, strongly suggests that not only the cytoskeleton but more specifically the neuronal outgrowth machinery is affected. This hypothesis is also supported by the signaling pathways that were found to be regulated: most of these components are known to affect neuronal cytoskeleton dynamics as well as growth cone motility, especially the 14-3-3 family of proteins (39, 40), the CRMP signaling pathway (41), and the Rho-GTPase signaling pathways (42). In line with the observed regulation of the Rho-GTPase signaling pathway, we found another molecule that is regulated in the CNS tissue of Nogo-A KO mice, cofilin, which has been suggested by Hsieh *et al.* (31) to be downstream of Nogo-A signaling. The Rho-GTPase signaling pathway can affect the phosphorylation state of LIMK1, which can phosphorylate and inactivate cofilin (32). We observed two spots being regulated for cofilin in the two-dimensional gel electrophoresis approach (0.79 (−1.27) and 1.70-fold, respectively) (Table 1), whereas the ICAT data showed only a slight down-regulation of its total level (Table 2). Western blot analysis in a separate set of animals confirmed the increase in cofilin phosphorylation but did not show significant changes in its total level, probably due to high interindividual variability. These data point to the potential regulation of cofilin activity through phosphorylation in the intact adult nervous system of Nogo-A KO mice. Therefore, the Rho-GTPase/LIMK1/cofilin signaling pathway is a candidate in the regulation of neuronal cytoskeletal proteins in the absence of Nogo-A signaling.

*Increased Growth Cone Motility in Nogo-A KO Neurons through the LIMK1/Cofilin Pathway*—The analysis of the observed regulated signaling pathways in our proteomic approach had highlighted the Rho-GTPase/LIMK1/cofilin signaling pathway as a potential, even if not unique, candidate in the regulation of neuronal cytoskeletal proteins in the absence of Nogo-A signaling. Our experiments further supported this: the Western blot analysis showed increased levels of phosphorylated LIMK1 as well as cofilin in the intact spinal cords of adult Nogo-A KO mice. Moreover, LIMK1 phosphorylation was up-regulated in growth cones of DRG neurons dissected from adult Nogo-A KO mice. LIMK1 phosphorylation depends on the activity of ROCK, regulated by GTP-bound Rho, and of PAK1, regulated by Rac and Cdc42. Interestingly, Nogo-A is already known to modulate RhoA activity. Our data confirm a role for Rho activation in Nogo-A-mediated neuronal cytoskeleton rearrangements, as an increase in activated GTP-bound Rho could be observed in growth cones of Nogo-A KO neurons. Cofilin is inactivated by phosphorylation at $Ser^3$ by

active LIMK and is known as an essential regulator of actin dynamics through its filament-severing activity (34, 39). Its high expression at the growth cone has pointed to its possible involvement in the regulation of growth cone motility: cofilin increased the length of neurite outgrowth when expressed in rat cortical neurons in primary cultures (43), suggesting that it plays a critical role in neurite extension and growth cone motility. Endo *et al.* (34) recently found that a cell-permeable cofilin fragment (S3 peptide) containing the $Ser^3$ phosphorylation site binds to and inhibits the endogenous LIMK1 activity. The resulting reduced endogenous phosphorylated cofilin levels in the growth cones suppressed growth cone motility and extension in chick DRG neurons, suggesting that LIMK1 stimulates neurite extension through its cofilin-phosphorylating activity. In addition, it has been shown that LIMK1 activation state can influence dendritogenesis (44). Because of all these numerous observations, the observed modulation of the LIMK1/cofilin pathway in the spinal cords of unlesioned adult Nogo-A KO mice and at the growth cones of Nogo-A KO adult neurons could influence growth cone morphology and motility and neurite outgrowth. In fact, we observed that growth cones of Nogo-A KO adult DRG neurons are larger and more motile compared with WT ones. Moreover, the increase in the growth cone area is due to an enlargement of lamellipodia but not of the microtubule-containing core of the growth cone, pointing to a key role of the actin cytoskeleton and to its modulation. The increase in growth cone motility translated in long-term cultures into a noticeably increased neuronal total outgrowth, as described previously (12). The specificity of the observed phenotype was confirmed by its reproducibility by antibody-mediated acute neuronal Nogo-A neutralization in WT adult DRG neurons and by its reproducibility in Nogo-A KO postnatal dissociated DRG neurons. These results point to neuronal Nogo-A as major contributor to the observed phenotype and highlight the specificity of the observed effects, which could be otherwise attributed to the regulation of compensating molecules like Nogo-B, which has been described to be highly up-regulated in Nogo-A KO mice (12).

More evidence of a direct link between the observed phenotype of increased growth cone motility and the observed regulation of the LIMK1/cofilin pathway was obtained by the fact that the presence of the S3 peptide, which activated cofilin by decreasing its phosphorylation, caused the reversion of the observed phenotype *in vitro* in Nogo-A KO growth cones: they moved at a lower speed, which was comparable with that of WT growth cones.

*Summary*—This study provides mechanistic insights into the function of neuronal Nogo-A in the unlesioned CNS and the related molecular signaling pathways. Our results suggest that Nogo-A might act as neuronal local growth suppressor in the intact nervous system both in adulthood and during development: its ablation causes modulation of Rho-GTP and of the LIMK1/cofilin pathway through phosphorylation regulation, which leads to actin cytoskeleton remodeling, increased growth cone motility, and neurite outgrowth in an intact system. In conclusion, we suggest that neuronal Nogo-A could play a role in the fine regulation of neuronal growth control through growth cone motility modulation in the intact adult as well as developing nervous system.

*Acknowledgments—We are grateful to F. Christ for animal facility management, S. Erb and Dr. V. Pernet for cell culture advice, R. Schoeb and E. Hochreutener for image processing, Dr. M. Hoechli and EMZ Zürich for technical advice and facilities for time-lapse video imaging, and the Functional Genomics Center of Zurich for support with the systems biology experiments. The RGC-5 cells were kindly provided by Dr. Krishnamoorthy.*

## REFERENCES

1. Fawcett, J. W. (2006) *Adv. Exp. Med. Biol.* **557,** 11–24
2. Schwab, M. E. (2004) *Curr. Opin. Neurobiol.* **14,** 118–124
3. Benowitz, L. I., and Yin, Y. (2007) *Dev. Neurobiol.* **67,** 1148–1165
4. Yiu, G., and He, Z. (2006) *Nat. Rev. Neurosci.* **7,** 617–627
5. Fabes, J., Anderson, P., Yanez-Munoz. R. J., Thrasher, A., Brennan, C., and Bolsover, S. (2006) *Eur. J. Neurosci.* **23,** 1721–1730
6. Figueroa, J. D., Benton, R. L., Velazquez, I., Torrado, A. I., Ortiz, C. M., Hernandez, C. M., Diaz, J. J., Magnuson, D. S., Whittemore, S. R., and Miranda, J. D. (2006) *J. Neurosci. Res.* **84,** 1438–1451
7. De Wit, J., and Verhaagen, J. (2003) *Prog. Neurobiol.* **71,** 249–267
8. Kaneko, S., Iwanami, A., Nakamura, M., Kishino, A., Kikuchi, K., Shibata, S., Okano, H. J., Ikegami, T., Moriya, A., Konishi, O., Nakayama, C., Kumagai, K., Kimura, T., Sato, T., Goshima, Y., Taniguchi, M., Ito, M., He, Z., Toyama, Y., and Okano, H. (2006) *Nat. Med.* **12,** 1380–1389
9. Pasterkamp, R. J., and Verhaagen, J. (2006) *Philos. Trans. R. Soc. Lond. B Biol. Sci.* **361,** 1499–1511
10. Cafferty, W. B., and Strittmatter, S. M. (2006) *J. Neurosci.* **26,** 12242–12250
11. Freund, P., Schmidlin, E., Wannier, T., Bloch, J., Mir, A., Schwab, M. E., and Rouiller, E. M. (2006) *Nat. Med.* **12,** 790–792
12. Dimou, L., Schnell, L., Montani, L., Duncan, C., Simonen, M., Schneider, R., Liebscher, T., Gullo, M., and Schwab, M. E. (2006) *J. Neurosci.* **26,** 5591–5603
13. Kim, J. E., Li, S., GranPré, T., Qiu, D., and Strittmatter, S. M. (2003) *Neuron* **38,** 187–199
14. Simonen, M., Pedersen, V., Weinmann, O., Schnell, L., Buss, A., Ledermann, B., Christ, F., Sansig, G., van der Putten, H., and Schwab, M. E. (2003) *Neuron* **38,** 201–211
15. Zheng, B., Ho, C., Li, S., Keirstead, H., Steward, O., and Tessier-Lavigne, M. (2003) *Neuron* **38,** 213–224
16. Huber, A. B., Weinmann, O., Brosamle, C., Oertle, T., and Schwab, M. E. (2002) *J. Neurosci.* **22,** 3553–3567
17. Wang, X., Chun, S. J., Treloar, H., Vartanian, T., Greer, C. A., and Strittmatter, S. M. (2002) *J. Neurosci.* **22,** 5505–5515
18. Mingorance-Le Meur, A., Zheng, B., Soriano, E., and del Rio, J. A. (2007) *Cereb. Cortex* **17,** 2375–2386
19. Aloy, E. M., Weinmann, O., Pot, C., Kasper, H., Dodd, D. A., Rulicke, T., Rossi, F., and Schwab, M. E. (2006) *Brain Cell Biol.* **35,** 137–156
20. Jin, W. L., Liu, Y. Y., Liu, H. L., Yang, H., Wang, Y., Jiao, X. Y., and Ju, G. (2003) *J. Comp. Neurol.* **458,** 1–10
21. Liu, Y. Y., Jin, W. L., Liu, H. L., and Ju, G. (2003) *Neurosci. Lett.* **346,** 153–156
22. Trifunovski, A., Josephson, A., Bickford, P. C., Olson, L., and Brené, S. (2006) *Neuroreport* **17,** 913–916
23. Nyatia, E., and Lang, D. M. (2007) *Res. Vet. Sci.* **83,** 287–301
24. Dodd, D. A., Niederoest, B., Bloechlinger, S., Dupuis, L., Loeffler, J. P., and Schwab, M. E. (2005) *J. Biol. Chem.* **280,** 12494–12502
25. Bareyre, F. M., Haudenschild, B., and Schwab, M. E. (2002) *J. Neurosci.* **22,** 7097–7110
26. Buffo, A., Zagrebelski, M., Huber, A. B., Skerra, A., Schwab, M. E., Strata, P., and Rossi, F. (2000) *J. Neurosci.* **20,** 2275–2286
27. Gianola, S., Savio, T., Schwab, M. E., and Rossi, F. (2003) *J. Neurosci.* **23,**

4613–4624
28. Gupta, N., Wollscheid, B., Watts, J. D., Scheer, B., Aebersold, R., and DeFranco, A. L. (2006) *Nat. Immunol.* **7,** 625–633
29. Han, M. H., Hwang, S. I., Roy, D. B., Lundgren, D. H., Price, J. V., Ousman, S. S., Fernald, G. H., Gerlitz, B., Robinson, W. H., Baranzini, S. E., Grinnel, B. W., Raine, C. S., Sobel, R. A., Han, D. K., and Steinman, L. (2008) *Nature* **451,** 1076–1081
30. Meijering, M., Jacob, E., Sarria, J. P., Steiner, P., Hirling, H., and Unser, M. (2004) *Cytometry* **58,** 167–176
31. Hsieh, S. H., Ferraro, G. B., and Fournier, A. E. (2006) *J. Neurosci.* **26,** 1006–1015
32. Bernard, O. (2007) *Int. J. Biochem. Cell Biol.* **39,** 1071–1076
33. Endo, M., Ohashi, K., Sasaki, Y., Goshima, Y., Niwa, R., Uemura, T., and Mizuno, K. (2003) *J. Neurosci.* **23,** 2527–2537
34. Endo, M., Ohashi, K., and Mizuno, K. (2007) *J. Biol. Chem.* **282,** 13692–13702
35. Grabham, P. W., Seale, G. E., Bennecib, M., Goldberg, D. J., and Vallee, R. B. (2007) *J. Neurosci.* **27,** 5823–5834
36. Medeiros, N. A., Burnette, D. T., and Forscher, P. (2006) *Nat. Cell Biol.* **8,** 215–226
37. Sachdev, P., Menon, S., Kastner, D. B., Chuang, J.-Z., Yeh, T.-Y., Conde, C., Caceres, A., Sung, C.-H., and Sakmar, T. P. (2007) *EMBO J.* **26,** 2621–2632
38. Tom, V. J., Steinmatz, M. P., Miller, J. H., Doller, C. M., and Silver, J. (2004) *J. Neurosci.* **24,** 6531–6539
39. Sarmiere, P. D., and Bamburg, J. R. (2004) *J. Neurobiol.* **58,** 103–117
40. Soosairajah, J., Maiti, S., Wiggan, O., Sarmiere, P., Moussi, N., Sarcevic, B., Sampath, R., Bamburg, J. R., and Bernard, O. (2005) *EMBO J.* **24,** 473–486
41. Arimura, N., Ménager, C., Kawano, Y., Yoshimura, T., Kawabata, S., Hattori, A., Fukata, Y., Amano, M., Goshima, Y., Inagaki, M., Morone, N., Usukura, J., and Kaibuchi, K. (2006) *Mol. Cell. Biol.* **25,** 9973–9984
42. Huber, A. B., Kolodkin, A. L., Ginty, D. D., and Cloutier, J. F. (2003) *Annu. Rev. Neurosci.* **26,** 509–563
43. Meberg, P. J., and Bamburg, J. R. (2000) *J. Neurosci.* **20,** 2459–2469
44. Lee-Hoeflich, S. T., Causing, C. G., Podkowa, M., Zhao, X., Wrana, J. L., and Attisano L. (2004) *EMBO J.* **23,** 4792–4801